CHAPTER III

RESULTS AND DISCUSSION

3.1 Synthesis and characterization of fluorophores

The synthesis of **F1** began with a Suzuki coupling reaction between methyl 4-iodosalicylate and bis-(pinacolato)diboron to obtain boronate ester **1**. This boronate ester was then reacted with dibromofluorene to obtain **2** followed by a treatment with a saturated KOH aqueous solution to afford **F1** in 71% yield after acidification using 6M HCl.

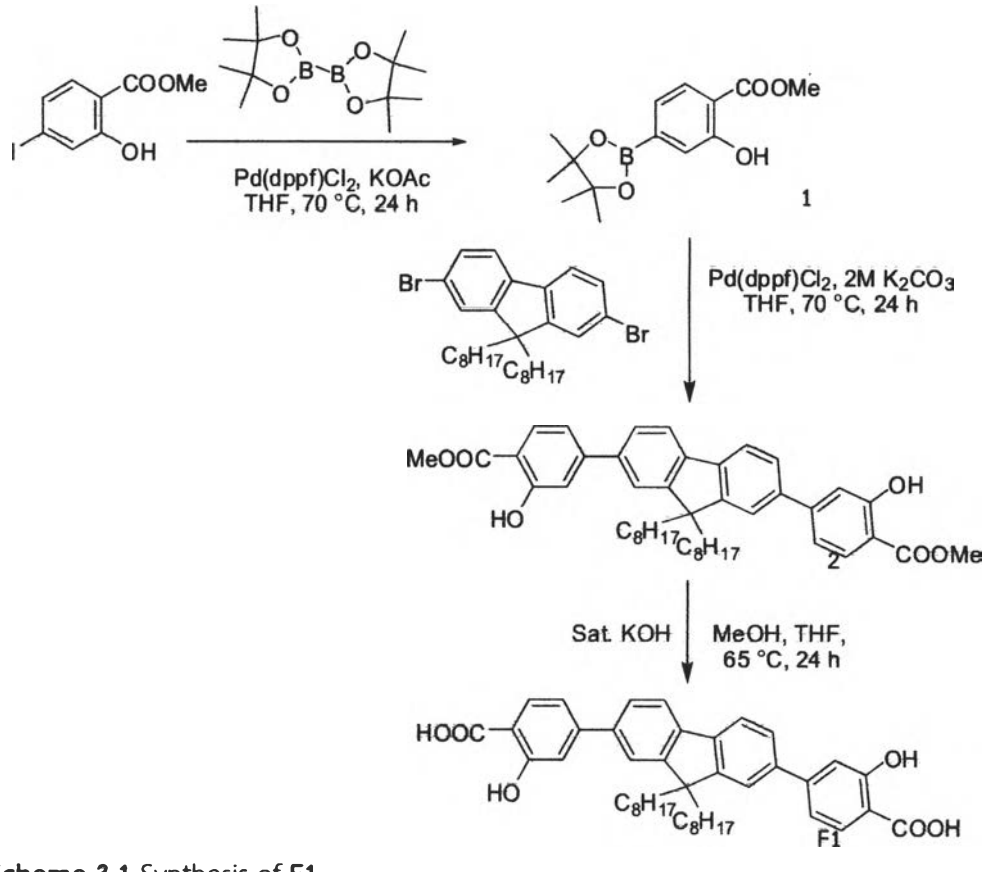

Scheme 3.1 Synthesis of **F1**

The ^{1}H NMR spectra of **1** and **2** in $CDCl_3$ and **F1** in DMSO-*d6* are shown in **Figure 3.1**. In the spectra of **1,** there are signals of tetramethyl dioxoboron and salicylate group that indicate a successful coupling of the two moieties. The absence of the methoxy group in **F1** suggested that the hydrolysis of the methyl salicylate group was successful.

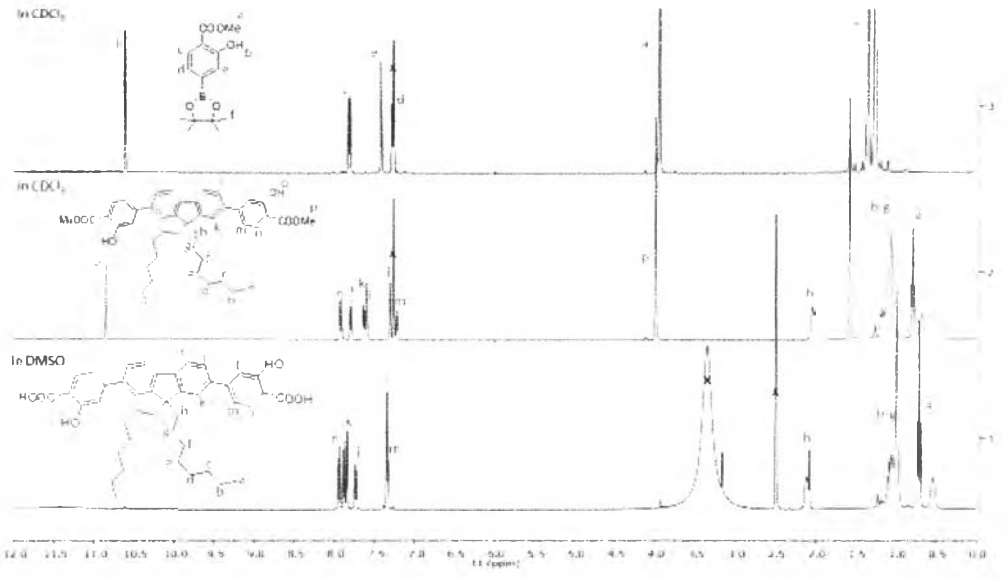

Figure 3.1 ^{1}H-NMR (400 MHz) of **1 and 2** in $CDCl_3$ and **F1** in DMSO-*d6*.

The ^{13}C-NMR spectrum of F1 (Figure A.4, see appendix) shows the carbon signals in the alkyl and aromatic region around 13-31 and 110-172 ppm, respectively.

Moreover, the analysis by MALDI-TOF mass spectrometry confirmed the structural composition of **F1** as a mass of 661.60 was found for this compound whose calculated exact mass is 662.36

Compound **3** was obtained by Sonogashira coupling between 2,7-dibromo-9,9-dioctyl-9H-fluorene and trimethylsilylacetylene. The desilylation to afford **4** was successfully performed using K_2CO_3. The Sonogashira coupling reaction between methyl 4-iodosalicylate and **4** gave rise to **5**, which was treated by saturated KOH to hydrolyze the ester group and produce **F2** in 87% yield (2 steps).

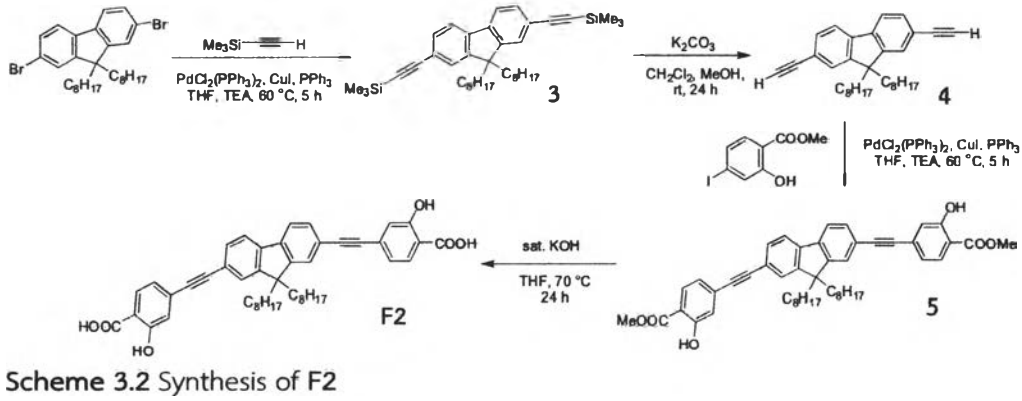

Scheme 3.2 Synthesis of F2

2905392820

ลงหมู่.....
เลขทะเบียน.....7228
วันเดือนปี.....

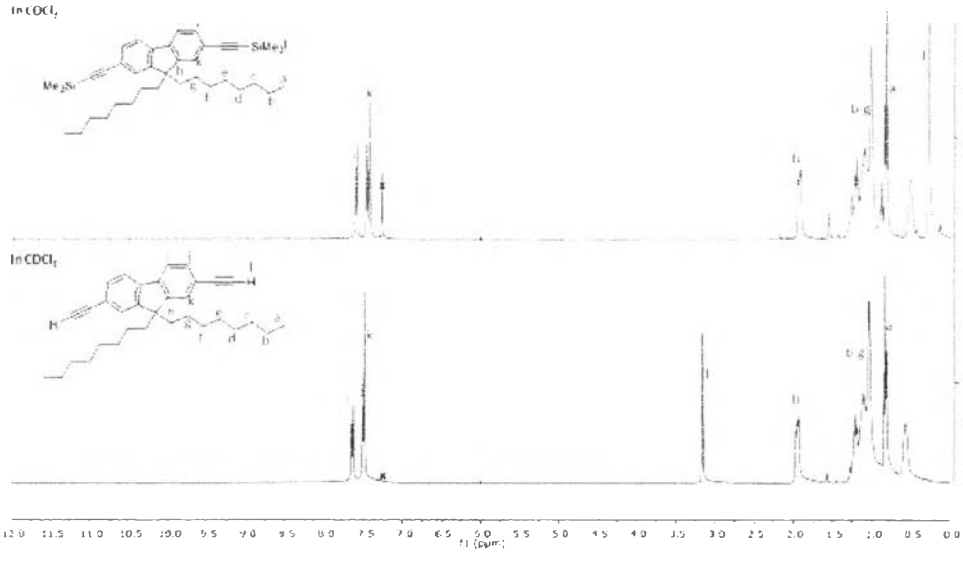

Figure 3.2 ^{1}H-NMR (400 MHz) of **3** and **4** in $CDCl_3$.

2905392820

Figure 3.2 shows ^{1}H-NMR of **3** and **4** in $CDCl_3$. The spectrum of **3** indicates a successful coupling reaction as the signal of trimethylsilylacetylene was observed. The absence of this trimethylsilylacetylene signal at 0.28 ppm and the presence of terminal alkyne peak at 3.16 ppm indicate a successful hydrolysis of **4**. The ^{1}H-NMR spectra of **5** in $CDCl_3$ and **F2** in DMSO-d6 are shown in **Figure 3.3**. The spectra of **5** display the signals of fluorine fragment (a-k) and salicylate group (l-p). The hydrolysis of the methyl group by saturated KOH was successful as the signal of methoxy group disappeared.

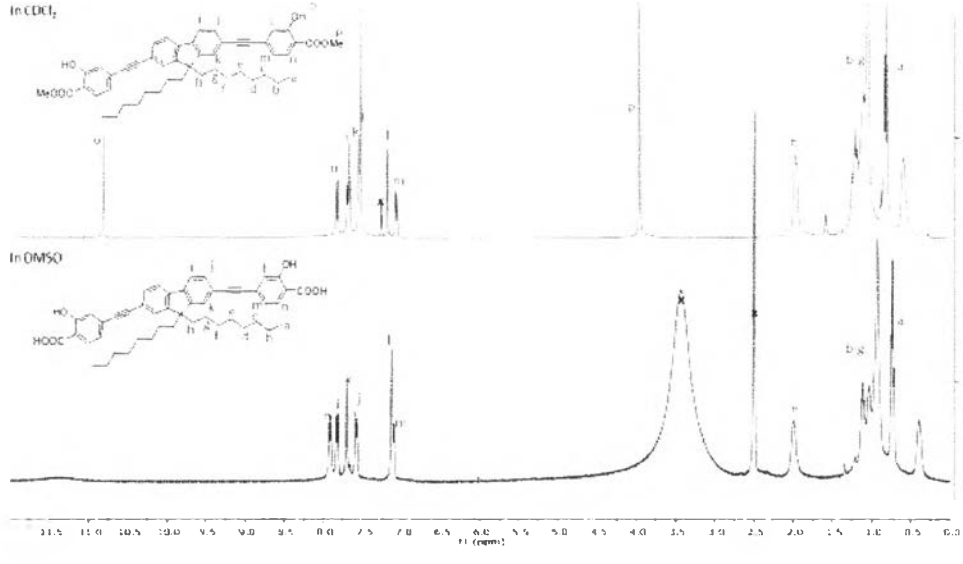

Figure 3.3 ^{1}H-NMR (400 MHz) of **5** in $CDCl_3$ and **F2** in DMSO-*d6*.

The ^{13}C-NMR spectrum of **F2** (Figure A.9, see appendix) indicates the presence of two acetylenic carbons resonate around 88-91 ppm, and the rest of the carbons signals show the alkyl and aromatic region around 13-31 and 110-172 ppm, respectively. Furthermore, the analysis by MALDI-TOF mass spectrometry confirmed the structural composition of **F1** as a mass of 709.67 was found for this compound whose calculated exact mass is 710.36

The fluorenone fragment in **F3** was prepared by air-oxidation reaction of 2,7-dibromo-9H-fluorene to obtain **6** in 97% yield. The Sonogashira coupling between **6** and trimethylsilylacetylene obtained **7**, followed by a base-catalyzed hydrolysis afforded **8** in moderate yield of 68% (2 steps). Another Sonogashira coupling and ester hydrolysis sequence provided **F3** in 60% yield (2 steps).

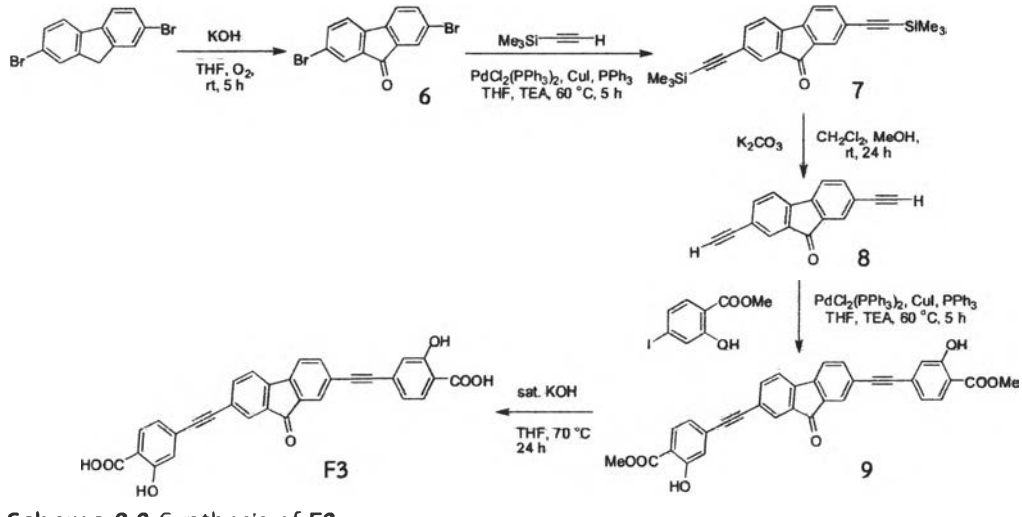

Scheme 3.3 Synthesis of F3

2905392820

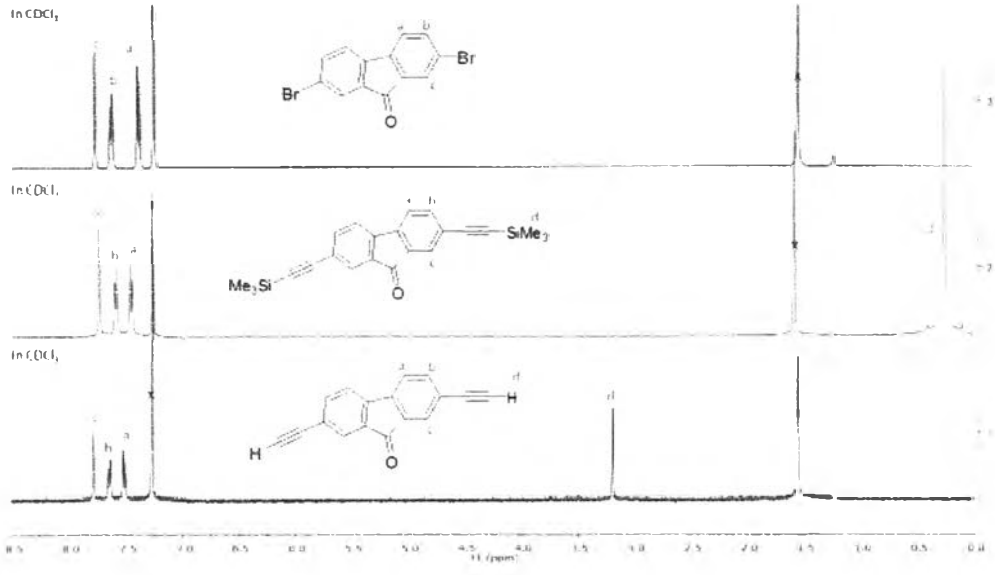

Figure 3.4 ^{1}H-NMR (400 MHz) of **6** **7** and **8** in $CDCl_3$.

2905392820

The ^{1}H-NMR spectra of **6** **7** and **8** in $CDCl_3$ are shown in **Figure 3.4**. NMR data of **6** are similar to that reported in literature [15]. The successful synthesis of **7** and **8** was evidenced by the signal of trimethylsilylacetylene in **7** and terminal alkyne in **8**. The Suzuki coupling reaction between fluorenone and methyl 4-iodosalicylate was successful resulting in both fluorenone and salicylate peaks in the ^{1}H-NMR spectra of **9**. The peak of methoxy group at 3.90 ppm is absent indicateing a complete base-catalyzed hydrolysis reaction to afford **F3** (**Figure 3.5**).

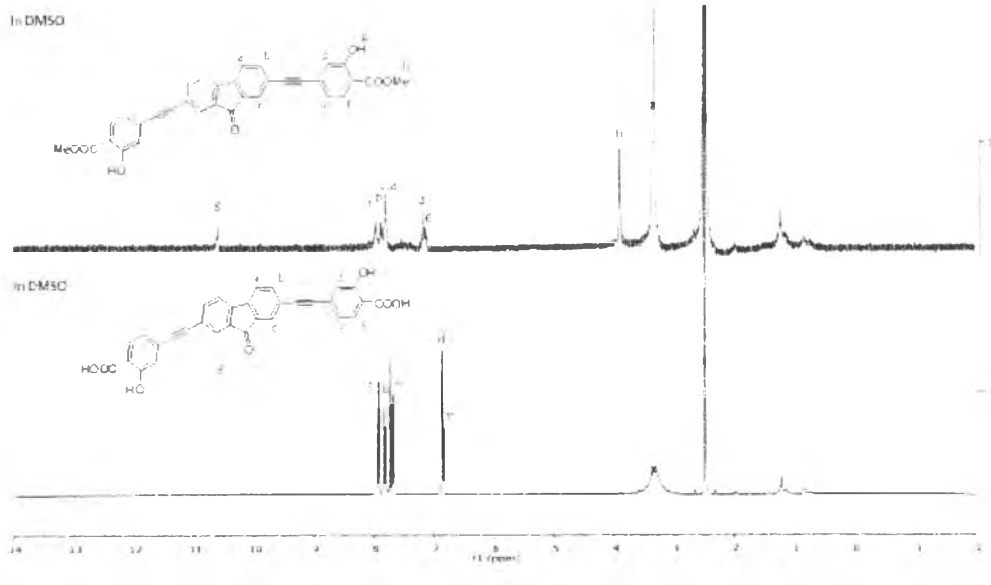

Figure 3.5 ^{1}H-NMR (400 MHz) of **3d** and **F3** in DMSO-*d6*

The ^{13}C-NMR spectrum of **F3** (Figure A.15, see appendix) also indicates the presence of the ketone and carboxylic acid carbonyl groups at 191.3 and 170.5 ppm, respectively. Two acetylenic carbons resonate around 88-91 ppm, and the rest of the carbons show signals in the aromatic region.

In addition, the analysis by high-resolution mass spectrometry confirmed the structural composition of **F3** as a mass of 499.17 was observed for this compound whose calculated exact mass is 500.09

In an attempt to perform a Pd-catalyzed cross-coupling reaction on dibromo dicyanomethylene derivative, a model compound **10** which was prepared in 79% yield from **6** and malononitrile was treated with boronate ester **1** under basic solution on K_2CO_3. This Suzuki coupling reaction was not successful because a competing hydrolysis of the dicyanomethylene group took place. Therefore, the labile dicyanomethylene group was installed as the last step of the synthesis of **F4**.

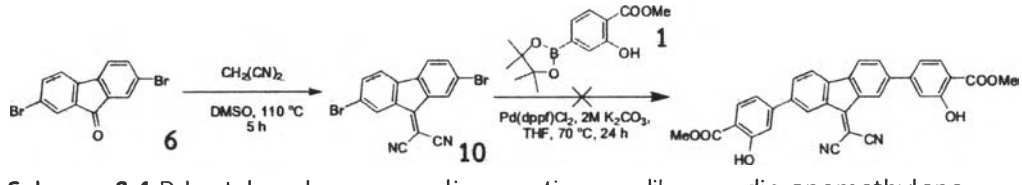

Scheme 3.4 Pd-catalyzed cross-coupling reaction on dibromo dicyanomethylene derivative

The reaction between **F3** and malononitrile in DMSO at 110 °C for 5 h produced dicyanomethylene **F4** in 61% yield after precipitation in reaction medium.

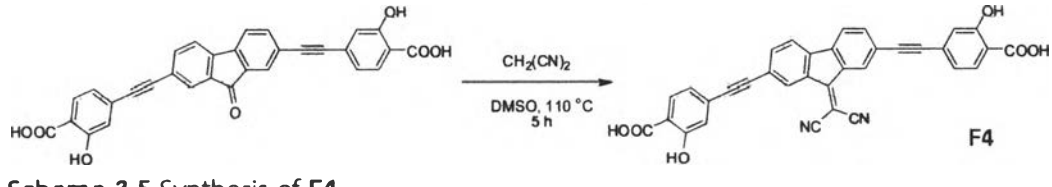

Scheme 3.5 Synthesis of **F4**

A comparison between the ^{1}H-NMR of **F3** and **F4** in DMSO-d6 are shown in Figure 3.6. Since dicyanomethylene is a stronger electron-withdrawing group than the ketone group, the substitution of dicyanomethylene at the 9-position should result in downfield shifts of the ^{1}H-NMR signals (**Figure 3.6**). Furthermore, the ^{13}C-NMR in Figure A.17 (see appendix) also verify the successful transformation from **F3** to **F4** as two additional carbon signals at 158.3 and 78.4 ppm from the dicyanomethylene unit emerge, whereas the ketone peak at 191 ppm disappears.

Furthermore, the analysis by MALDI-TOF mass spectrometry confirmed the structural composition of **F4** as a mass 550.26 of was found for this compound whose calculated exact mass is 548.10

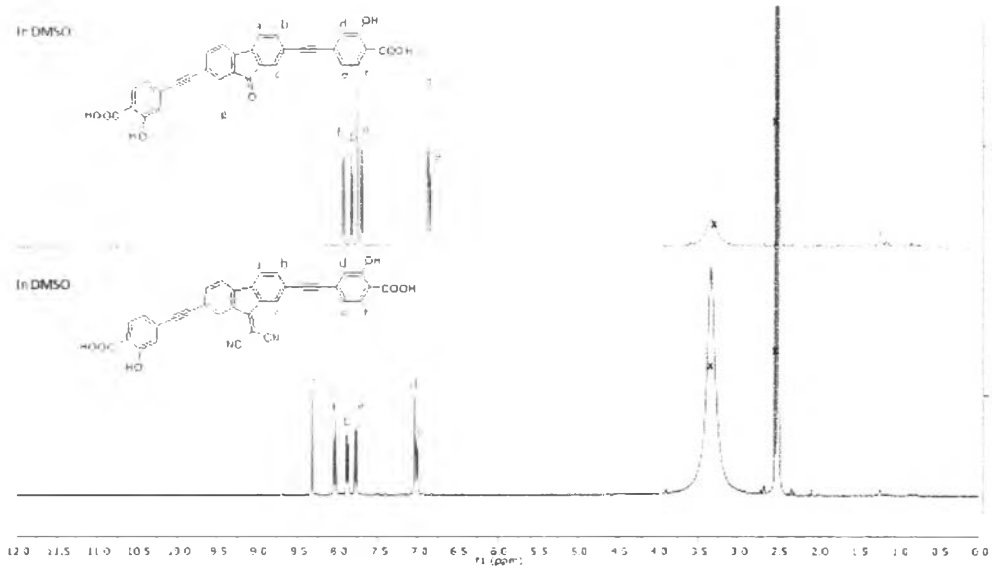

Figure 3.6 ^{1}H-NMR (400 MHz) of **F3** and **F4** in DMSO-*d6*

3.2 Photophysical properties

The photophysical properties of the four fluorophores (**F1-F4**) in phosphate buffer saline (PBS) pH 8.0 are shown in **Table 1** and **Figure 3.7**.

Table 3.1 Photophysical properties of **F1-F4** in PBS (10 mM, pH 8.0).

Cmpd.	Absorption		Emission		Stokes shift (nm)
	λ_{ab} (nm)	Log ε	λ_{em} (nm)	Φ (%)[a]	
F1	323	4.60	430	2.7	107
F2	330	4.55	420	4.4	90
F3	304	4.59	-	-	
	354	4.46			
F4	323	4.29	-	-	
	378	3.96			

[a]Quinine sulfate in 0.1 M H_2SO_4 (Φ = 0.54) was used as the standard.

2905392820

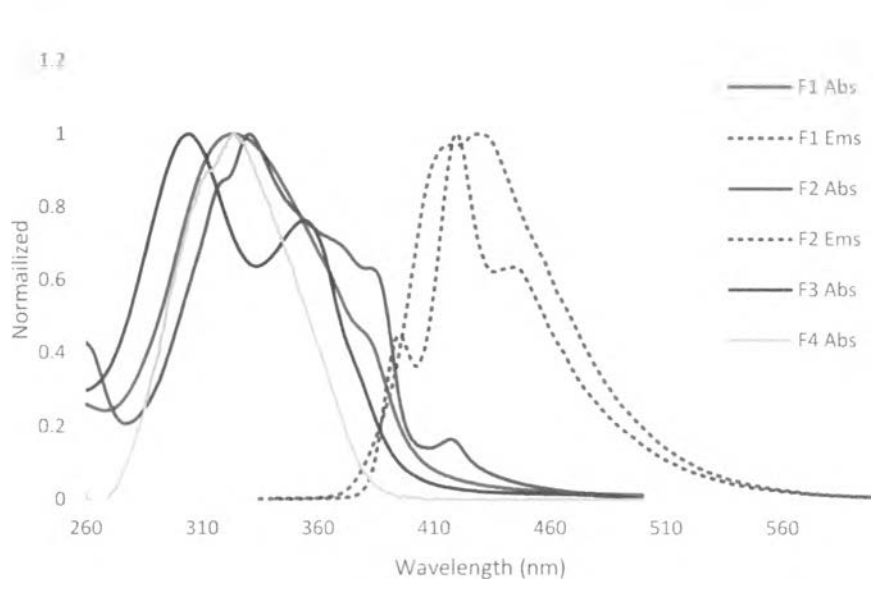

Figure 3.7 Normalized absorption of **F1**-**F4** and emission spectra of **F1**-**F2** in 10 mM phosphate buffer saline pH 8.0

From **Figure 3.7**, **F1** and **F2** show similar photophysical properties with the maximum absorption peak around 323-330 nm and maximum emission peak around 420-430 nm. From the narrower Stokes shift in **F2** compared to **F1**, it could be justified that the presence of ethynyl groups resulted in the excited state with a relatively similar geometry as in the ground state. Without the ethynyl group, the pi-systems of the salicylate and the fluorene groups in **F1** may not be completely overlapped due to steric hindrance. Upon excitation by radiation, the excited state of **F1** may have a different geometry such as those with the two photo active units on the same plane with full conjugation (**Figure 3.8**).

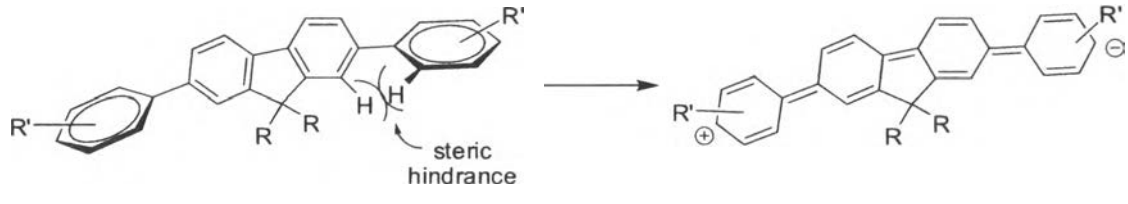

Ground state geometry **Excited state geometry**

Figure 3.8 Proposed geometry change in **F1**

For absorption spectrum of **F3**, there are peaks at 304 and 354 nm which corresponded to the characteristic peaks for salicylic acid and fluorenone, respectively. This is also the case for this absorption spectrum of **F4** which exhibits to distinct peaks

at 323 and 378 nm, albeit in a more combined manner. These data suggested that there are more electronic communication between the fluorene and ethynylsalicylate in **F4** as compared to **F3**. The fluorescence analysis revealed that both **F3** and **F4** are non-emissive materials, which may cause by several factors such as the n-π PET from fluorenone part in **F3** [18] and the ICT effect on the salicylate and the dicyanomethylene fluorene in **F4** (**Figure3.9**) [19, 20].

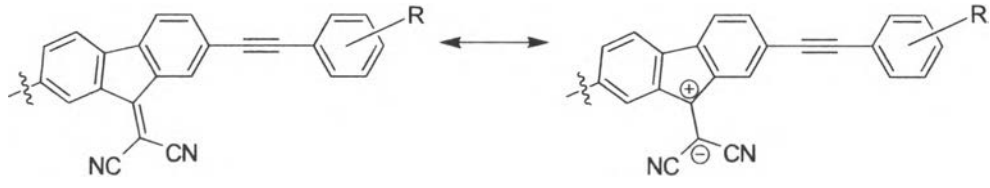

Figure 3.9 Proposed charge tranfers mechnism of **F4**

3.3 Metal ion sensor

To investigate the selectivity towards metal ions, the fluorescence responses of **F1** and **F2** (10 μM in pH 8.0 PBS) in the presence of various metal ions (100 μM) were observed. Data from **Figure 3.10** and **3.11** suggested that **F1** showed no particular selectivity towards any of the 17 metal ions, including Cu^{2+}, Fe^{2+}, Pb^{2+}, Hg^{2+}, Fe^{3+}, Hg^{+}, Zn^{2+}, Cr^{3+}, Co^{2+}, Ni^{2+}, Mn^{2+}, Ag^{+}, Al^{3+}, Na^{+}, Au^{3+}, Cd^{2+} and Ca^{2+}.

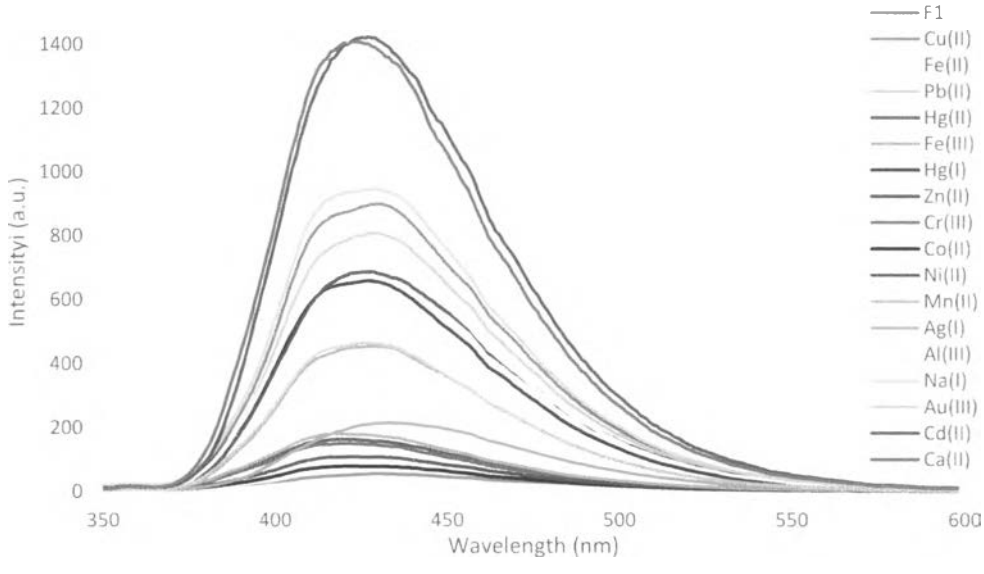

Figure 3.10 Fluorescence spectra of **F1** (10 μM) in the presence of 17 metal ions (100 μM) in PBS (10 mM, pH 8.0)

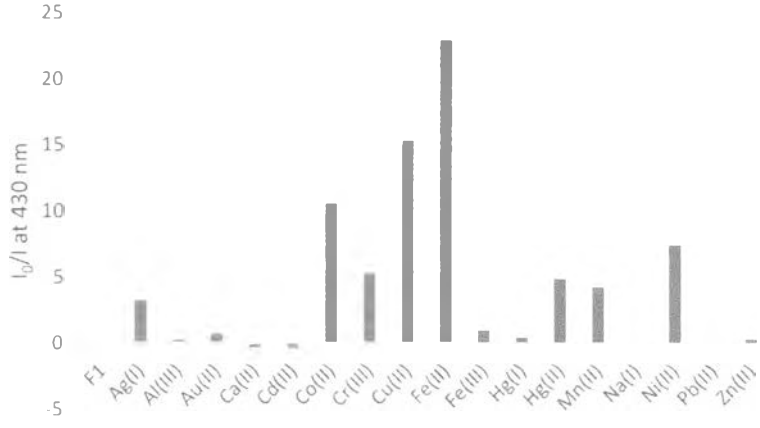

Figure 3.11 Fluorescence quenching of **F1** and (10 μM) by various metal ions (100 μM) in PBS (10 mM, pH 8.0)

However, the fluorescence signal of **F2** can be selectively quenched by the addition of Cu^{2+} and Fe^{2+} ions, with a slightly higher sensitivity for Fe^{2+} (**Figure 3.12** and **3.13**). This selectivity may result from the preferred complexation towards those two ions. [13].

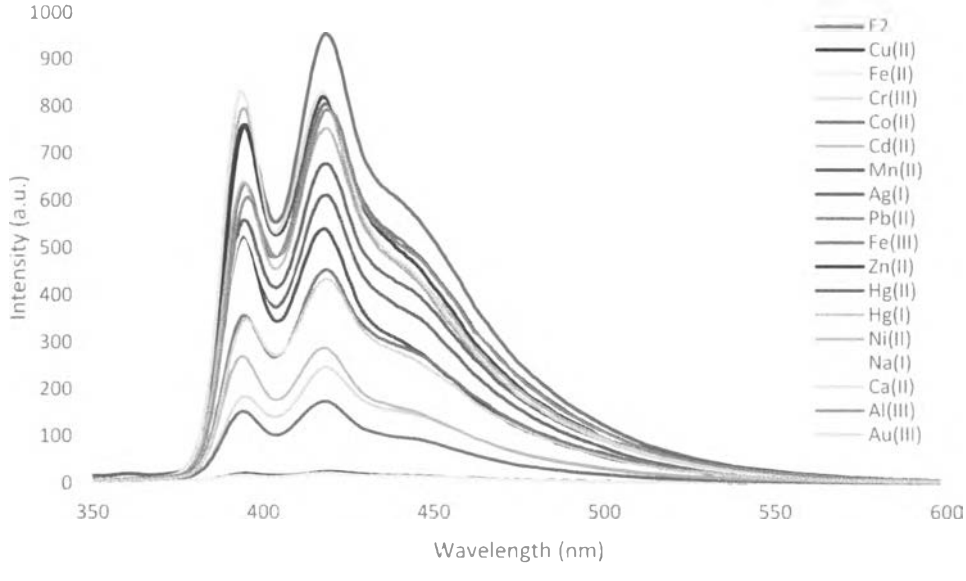

Figure 3.12 Fluorescence spectra of **F2** (10 μM) in the presence of 17 metal ions(100 μM). in PBS (10 mM, pH 8.0)

2905392820

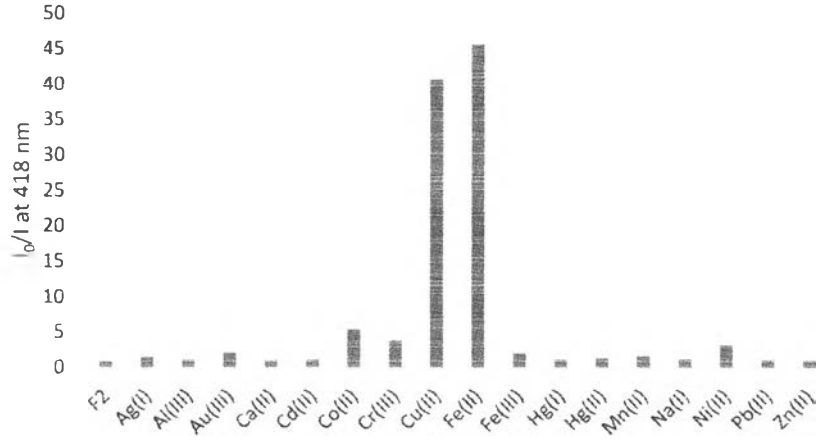

Figure 3.13 Fluorescence quenching of **F2** and (10 μM) by various metal ions (100 μM) in PBS (10 mM, pH 8.0)

The Stern-Volmer plots between I_0/I of **F2** with concentration of Cu^{2+} and Fe^{2+} are showed in Figure 3.11. The Stern-Volmer constants (K_{sv}) which are determined from slopes indicated that the quenching efficiencies are $2.14x10^6$ and $6.31x10^6$ M^{-1} for Cu^{2+} and Fe^{2+}, respectively (**Figure 3.14**).

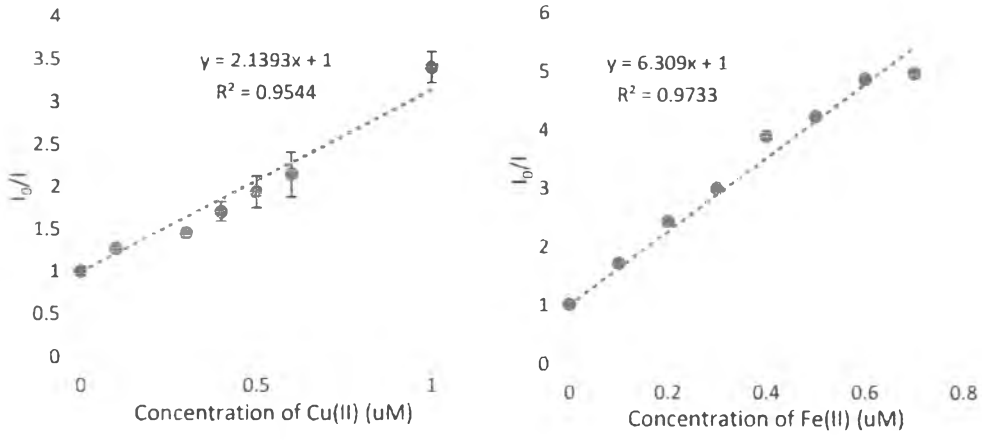

Figure 3.14 The Stern-Volmer plots of fluorescence quenching of **F2** (1 μM) by Cu^{2+}(left) and Fe^{2+}(right)

3.4 Surfactant enhancement

Previous literatures [11, 13] have reported the addition of surfactant can enhance the fluorescence signal of this class of compounds. In this work, the cationic (CTAB and DTAB), anionic (SDS and SDC), and non-ionic (Triton X-100, Brij-58 and Tween-20) were selected for the study. The fluorescence responses of **F2** in the presence of various surfactants are shown in **Figure 3.15** and **Figure 3.16**. It was found

that the initial fluorescence intensity could be enhanced the most by the non-ionic surfactants, while the effects of both cationic and anionic surfactants were not prominent. It should be noted that the concentrations of all surfactants used in this set of experiments were below the critical micelle concentration (CMC) of each surfactants. Therefore, the signal enhancement may not be due to the micellar effect but it could result from the overall polarity change of the medium caused by the surfactants which facilitate the deaggregation of the fluorphore.

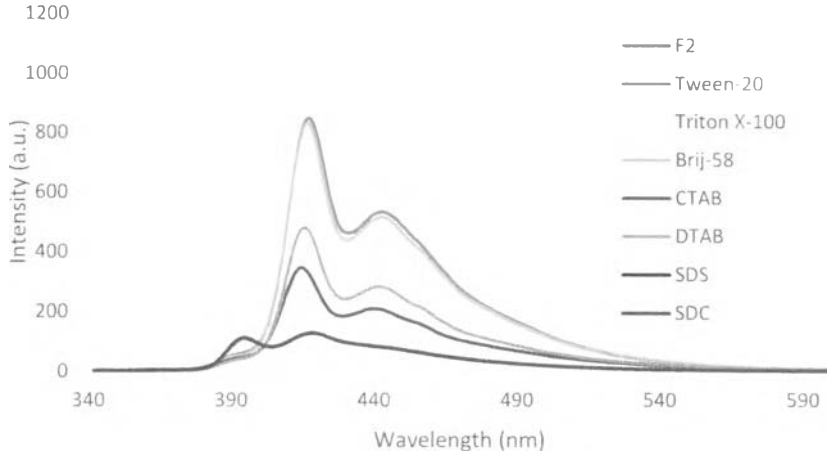

Figure 3.15 Fluorescence spectrum of **F2** (10 μM) towards various surfactant (40 μM)

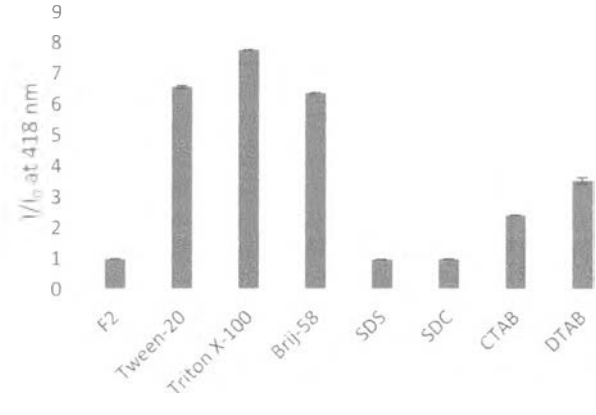

Figure 3.16 Enhancement efficient of various surfactants with F2

Next, this group of surfactants was incorporated into the sensing system and the quenching efficiencies (I_0/I) of **F2** by Cu^{2+} were measured (**Figure 3.17**). Of all non-ionic surfactants, it is apparent that Triton X-100 provided the highest sensitivity, However, the effect of this surfactant on sensitivity was not significant as the I_0/I value was similar to that obtained from the system without surfactant (**Figure 3.18**).

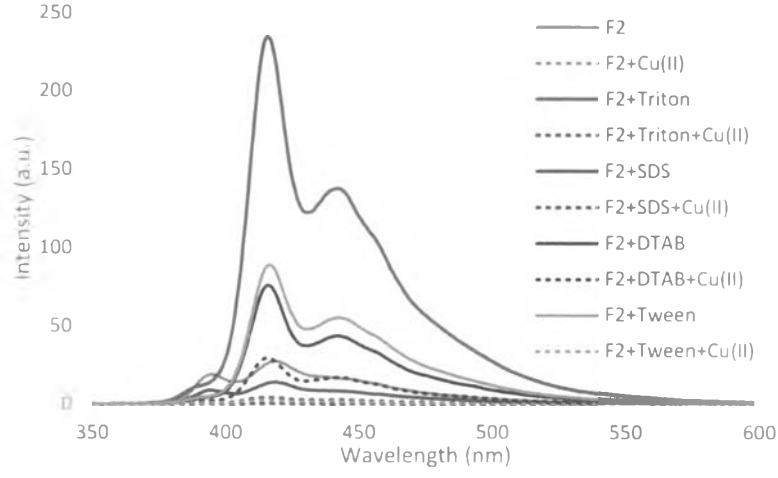

Figure 3.17 Effects of various surfactants on fluorescent signal of **F2** and its responses towards Cu^{2+}

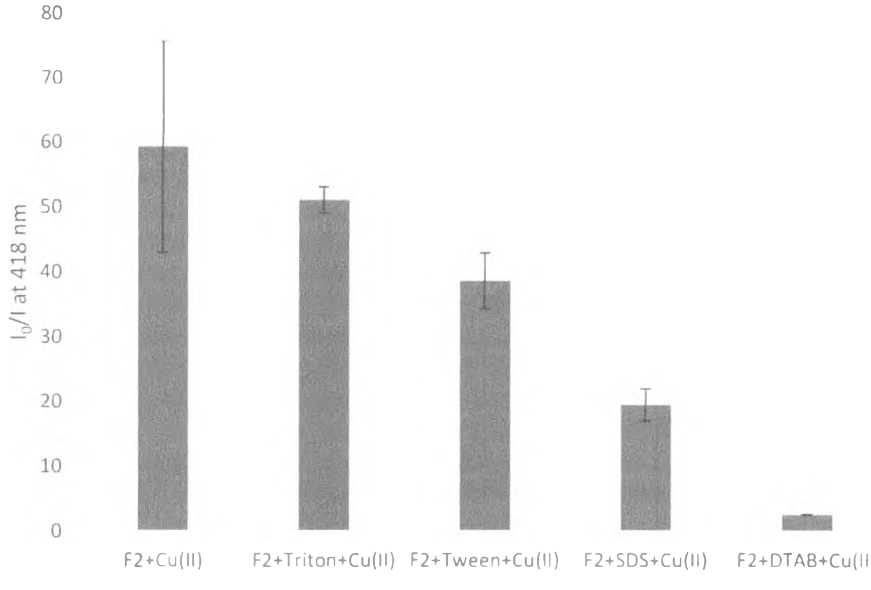

Figure 3.18 Quenching efficiencies of **F2** with Cu^{+2} under various surfactants

Interestingly, the addition of Triton X-100 could improve the selectivity of **F2** towards Cu^{2+} over Fe^{2+}. As shown in **Figure 3.19**, the use of Triton X-100 at 30-40 μM could enrich the selectivity towards Cu^{2+} over Fe^{2+} from 1.1 to 6.0. This selectivity improvement may cause by the preferred complexation between the glycol units that is Lewis base in Triton X-100 and the more Lewis acidic Fe^{2+} ion. To demonstrate that the incorporation of this surfactant will not interfere with the selectivity towards other metal ions, another series of experiment were carried out (**Figure 3.19** and **Figure3.20**)

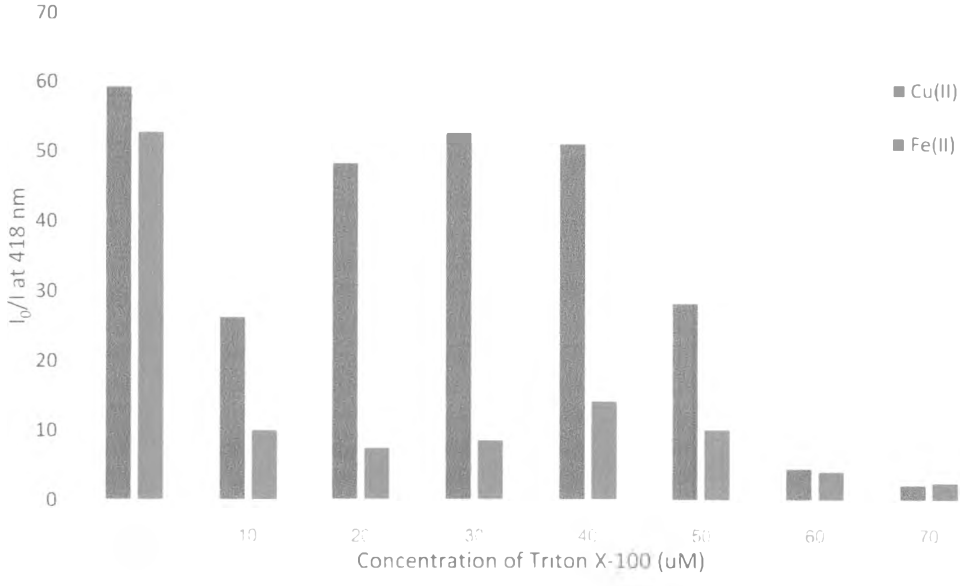

2905392820

Figure 3.19 Quenching efficiencies of **F2** by Cu^{2+} and Fe^{2+} under various concentration of Triton X-100

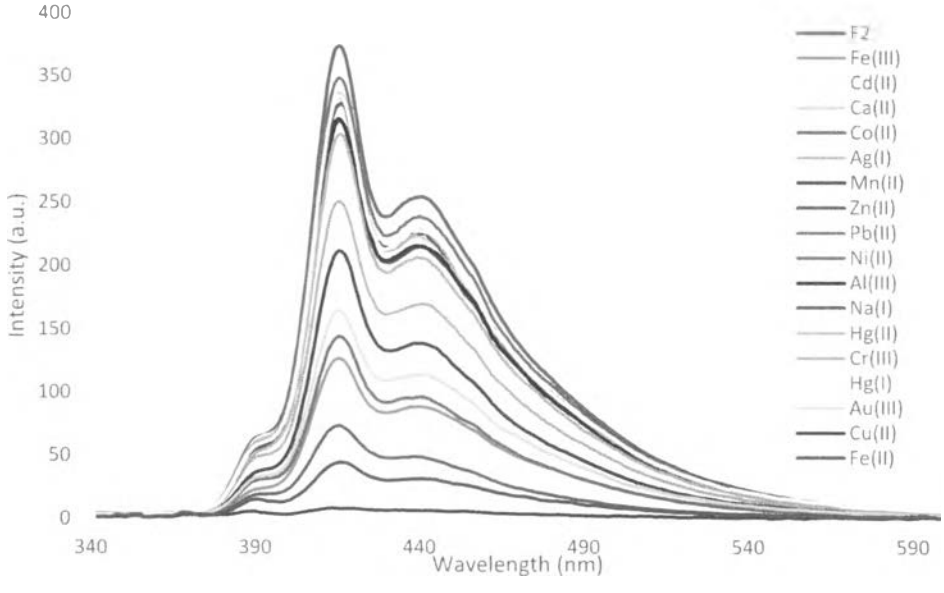

Figure 3.20 Fluorescence signals response of **F2** with Triton X-100 towards various metal ions

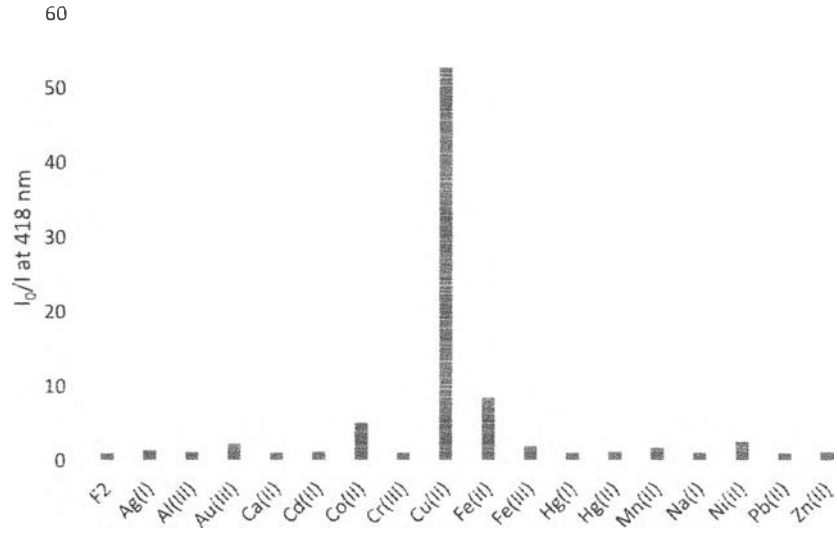

Figure 3.21 Bar chart shows fluorescence quenching of **F2** with Triton X-100 towards various metal ions

2905392820

The interference of other metal ions on the sensing of Cu^{2+} by **F2** were also investigated. **Figure 3.21** shows that other metal ions cannot interfere the quenching efficiency of **F2**, even when the concentration of foreign ions was 10-times higher than that of Cu^{2+}. A new Stern-Volmer plot of **F2** with Cu^{2+} under the conditions with surfactant shows a quenching constant (K_{sv}) of 4.08×10^6 M^{-1} which corresponds to a detection limit at three-times-noise of 1.47 ppb (**Figure 3.22**)

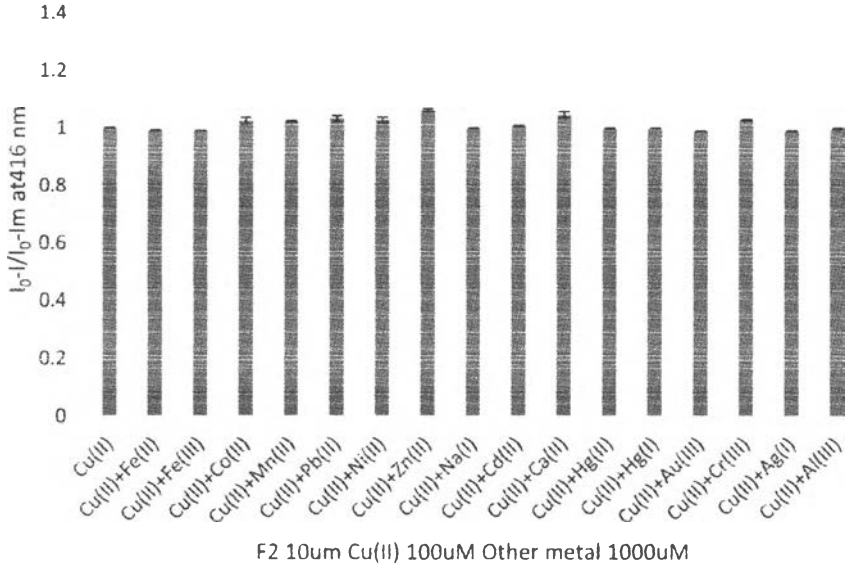

Figure 3.22 Fluorescence intensity ratio of **F2** (I_0-I/I_0-I_M) in presence Cu^{2+} and another metal ions

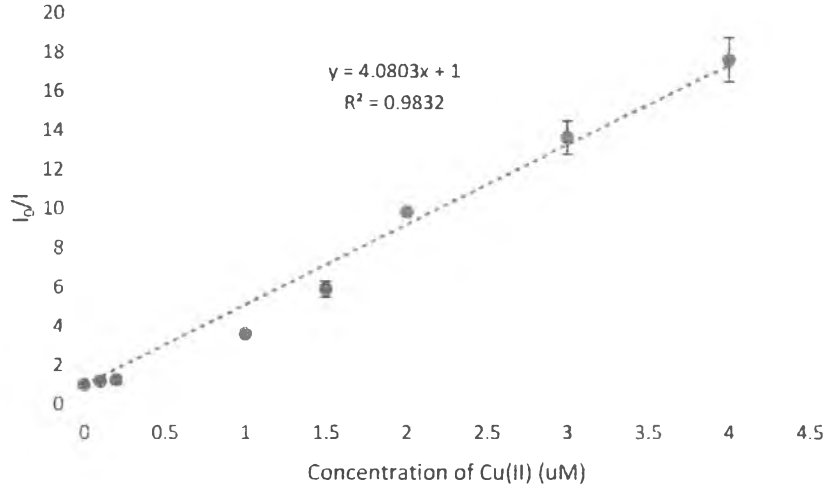

Figure 3.23 Stern-Volmer plot of fluorescence quenching of **F2** with Triton X-100 by Cu^{2+}

3.5 Indication of Cu^{2+}-**F2** complexation; an EDTA test

The complexation between salicylate and Cu^{2+} has been well established [10-13]. In order to prove the fluorescence quenching in our system was caused by the complexation of the salicylate unit in **F2** with Cu^{2+}, a solution of disodium

ethylenediaminetetraacetic acid (EDTA) which is a strong chelator for many transition metal ions was added. The recovery of fluorescence intensity of **F2** after the addition is a good indicator that our sensing mechanism involves a static energy transfer (**Figure 3.23**).

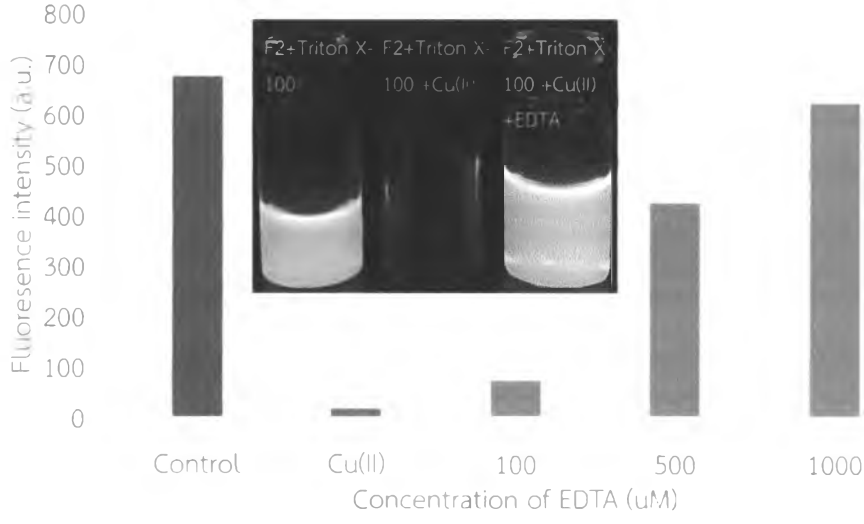

Figure 3.24 Effect of EDTA on recovery fluorescence intensity, inset: photogenic of F2 with Triton X-100 (left), photogenic of F2 with Triton X-100 after Cu^{2+} was added, and photogenic of addition of EDTA.

3.6 Paper-based sensor

To demonstrate a simple analytical technique for Cu^{2+} using **F2** [13, 21, 22], 1 μL of Cu^{2+} solutions at various concentration (20-500 μM) were dropped onto a piece of filter paper yielding spots of Cu^{2+} at 20-500 pmol, respectively. After the spots were allowed to dry at ambient temperature, solutions of **F2** in THF at concentration between 25-100 μM were dropped onto the same positions. **Figure 3.24 (top)** shows that **F2** can be used as a naked-eye sensor for Cu^{2+} of 40 pmol when the concentration of **F2** is 0.250 μM (correspond to 0.250 nmol). However, this solid-state detector cannot be applied under a surfactant environment, therefore, a similar selectivity towards Fe^{2+} was also observed (**Figure 3.24 (bottom)**).

2905392820

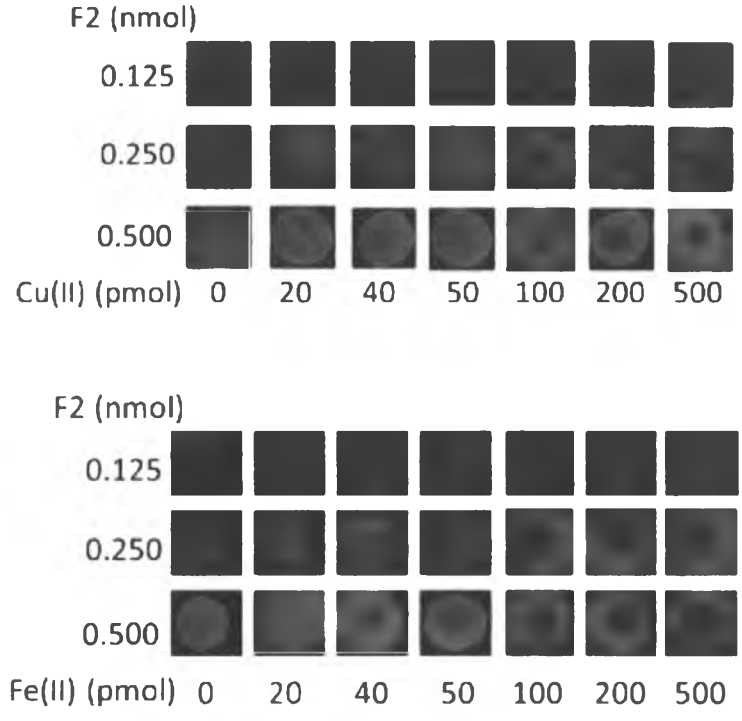

Figure 3.25 Photogenic of **F2** use as paper-based sensor for detection Cu^{2+} (top) and $F2^{2+}$ (bottom).

2905392820